ELSEVIER

Catalysis Today 40 (1998) 333–342

CATALYSIS TODAY

Fast catalytic oxidation of phenol in supercritical water

Xiang Zhang, Phillip E. Savage*

Department of Chemical Engineering, The University of Michigan, Ann Arbor, MI 48109-2136, USA

Abstract

The catalytic oxidation of phenol in water over a commercial oxidation catalyst, CARULITE 150, was investigated in a fixed bed flow reactor at 250 atm and temperatures from 380°C to 430°C. The phenol and oxygen concentrations at the reactor entrance varied between 0.070 and 1.24 mmol/l, and 9.60 and 39.6 mmol/l, respectively. The reaction conditions produced phenol conversions and selectivities to CO_2 much higher than those produced by non-catalytic oxidation. The kinetics of phenol disappearance and of CO_2 formation were both roughly first-order, and the activation energies were 31 and 47 kcal/mol, respectively. The catalyst did not undergo continuous deactivation during the catalytic oxidation, but rather maintained a high activity even after several days of continuous operation.

Keywords: Supercritical water; Kinetics; Deactivation

1. Introduction

Supercritical water oxidation (SCWO) is an emerging ''green'' technology for the destruction of organic compounds in industrial wastewater streams [1]. The SCWO process takes advantage of the unique properties of supercritical water (SCW), which brings together organic compounds, water, and oxygen (or air) in a single phase, and completely oxidizes organic waste materials to H_2O and CO_2. The first commercial facility employing the SCWO process became operational in 1994 [2,3], with operating temperatures as high as 650°C and pressures as high as 250 atm. Although operating at lower temperatures and pressures is clearly desired for industrial processes, the oxidation reactions at lower temperatures (around 400°C) are slow and produce numerous byproducts from incomplete oxidation [4–11].

One approach to overcome these problems is to perform catalytic oxidation reactions in SCW. Heterogeneous catalytic oxidation has been well studied in subcritical water [12–22]. This process is referred as catalytic wet air oxidation. Recently, studies of heterogeneous catalytic SCWO of model organic pollutants have demonstrated its potential advantage over non-catalytic SCWO in destroying organic wastes. Several groups of researchers reported that the use of heterogeneous catalysts for the oxidation of model organic compounds (including phenol) led to higher conversion and higher CO_2 selectivity at much shorter contact time and significantly lower temperatures (380–390°C) [23–26]. These studies also revealed that in most cases there was less leaching of metal ions from the catalysts in SCW than in subcritical water. Catalyst dissolution is a common drawback of catalytic wet air oxidation processes.

*Corresponding author. Tel.: 001 3137643386; fax: 001 3137630459; e-mail: psavage@umich.edu

0920-5861/98/$32.00
PII S0920-5861(98)00062-5

Although the potential advantages of catalytic SCWO have clearly been identified, there have been few studies of the catalytic SCWO kinetics and catalyst activity maintenance. There is a gap in the literature regarding the kinetics of catalytic SCWO of model organic compounds, especially compared to that already known about traditional non-catalytic SCWO. Knowledge of the reaction kinetics is important and helpful for preliminary design and economic evaluation of commercial-scale catalytic SCWO processes. In this study, we report the kinetics for the oxidation of phenol over CARULITE 150, a commercial oxidation catalyst from Carus Chemical.

2. Experimental

All experiments were performed in a tubular flow reactor that can be approximated as operating isothermally, isobarically and in plug-flow. The details of the flow reactor system were given previously [4]. In our study, a dilute aqueous solution of H_2O_2 is loaded into a pressure vessel and then blanketed with 600 psi of helium. An aqueous solution of phenol is loaded into a separate pressure vessel and likewise blanketed with 600 psi of helium. The aqueous solutions in the feed tanks form two feed streams, which are pressurized and pumped through preheat lines and then the reactor using two Eldex model AA-100-S micrometer pumps. During the preheating, H_2O_2 completely decomposed into O_2 and water. That decomposition was complete and was verified experimentally. The two streams are preheated separately in two 1/16 in. (1.6 mm) OD feed lines before being mixed in a Hastelloy C-276 cross which was fitted with a thermocouple. The reaction temperatures reported in this study are those detected by this thermocouple. The mixed feed streams then entered the reactor, which is assembled from 1/4 in. stainless steel Swagelok tube fittings (a union and two port connectors). A Hastelloy porous disk with up to 100 μm openings was placed at each end to keep the catalyst inside the union. The entire reactor assembly (including preheater line, mixing cross and reactor) was housed in a temperature-controlled Techne model SBL-2 fluidized sand bath that maintains isothermality to within 1°C.

Upon leaving the heated zone of the sand bath, the reactor effluent was cooled in two consecutive tube-in-tube heat exchangers and then depressurized in a Tescom model 44 back pressure regulator. The exiting stream was separated into gas and liquid phases (at ambient conditions) in a liquid trap. These two phases were assumed to be in equilibrium, and Henry's law was used to calculate the amount of CO and CO_2 dissolved in the liquid phase. The gas flow rate was measured with a bubble meter at the outlet of the system, and the gas stream was sent to an on-line gas chromatograph (GC) equipped with a thermal conductivity detector for analysis. The liquid flow rate was determined by measuring the volume collected in a graduated cylinder within a fixed time period, and samples of the liquid phase were retained for analysis.

The gaseous reactor effluent was analyzed by a Hewlett Packard model 5890 GC with a Supelco 10 ft by 1/8 in. OD stainless steel column packed with 100/120 mesh Carbosieve S-II. A 10-port Valco valve injected a 0.5 ml sample into the column and helium flowing at 20 ml/min served as the carrier gas. The oven temperature program was 35°C for the first 7 min, and then a ramp of 16°C/min up to 225°C. Detector response factors for CO_2 and CO were determined experimentally using standard gases.

A reverse-phase high-performance liquid chromatograph with a Supelco C18 column was used to determine the concentration of phenol in the liquid effluent samples. Analyses were performed isocratically with a mobile phase of acetonitrile and water (30:70 by volume). The mobile phase flow rate was 1 ml/min and the UV absorbance at a wavelength of 210 nm was monitored.

Higher molecular weight products of incomplete oxidation, which are present in much lower concentrations than phenol, were extracted from the aqueous effluent with dichloromethane. After concentrating the dichloromethane solution, the products were qualitatively analyzed by capillary column gas chromatography with a mass spectrometric detector (GC–MS). Details of the procedure were given previously [4–10].

The CARULITE 150 catalyst used was obtained from Carus Chemical. The active ingredients are 45–60% MnO_2 and 1–3% CuO, which are supported on amorphous Al_2O_3. The pellets obtained were ground to powders and separated by size. Particles within the size range 0.12–0.25 mm (or 60/120 mesh) were used to ensure that they would not go through the porous

disk with 100 μm opening. All experiments except for the deactivation studies were conducted using fresh catalyst. The catalyst was pretreated overnight by flowing a supercritical water stream carrying just oxygen through the reactor.

3. Experimental results

All experiments were conducted at 250 atm, most of them around 385°C. The phenol and oxygen concentrations at the reactor entrance varied between 0.070 and 1.24 mmol/l, and 9.60 and 39.6 mmol/l, respectively. Table 1 summarizes all the experimental conditions and results, including phenol conversions and the yields of CO_2 and CO. These yields were calculated as the molar flow rate of CO_2 (or CO) in the reactor effluent divided by six times the molar flow rate of phenol into the reactor. The phenol conversions are always greater than 70%. In addition, the selectivity to complete oxidation, which is calculated as the ratio of the yield of CO_2 to the phenol conversion, ranges from 52% to essentially 100%. It is generally higher than that obtained from the non-catalytic SCWO of phenol at comparable temperatures [4–11].

Due to this higher selectivity to CO_2 formation there must be a smaller amount of byproducts formed than from non-catalytic SCWO. This expectation was confirmed by a GC–MS analysis of the liquid effluent from run 6. This analysis revealed the presence of 2,5-cyclohexadiene-1,4-dione and trace amounts of 2- or 4-phenoxyphenol as products of incomplete oxidation. Dibenzo-*p*-dioxin, dibenzofuran, 2-dibenzofuranol, etc., which are produced as intermediate products from the non-catalytic SCWO of phenol [4–11], were not detected here. This difference suggests that catalytic SCWO involves different and faster pathways so that the non-catalytic dimerization pathway is suppressed. 2,5-Cyclohexadiene-1,4-dione was also identified as a major intermediate product during catalytic wet air oxidation of phenol [19]. Thus, it appears that catalytic SCWO likely follows reaction pathways similar to those of catalytic wet air oxidation.

We calculated the phenol conversion and CO_2 yield that would be produced by non-catalytic SCWO under the present experimental conditions on the basis of the rate laws previously established [4–10]. These calculations show that the non-catalytic contributions to the phenol conversion and the CO_2 yield are only a small portion of the experimentally observed values. Fig. 1 shows that the amount of the CO_2 yield produced experimentally that can be attributed to non-catalytic oxidation reactions is always less than 6% of the total.

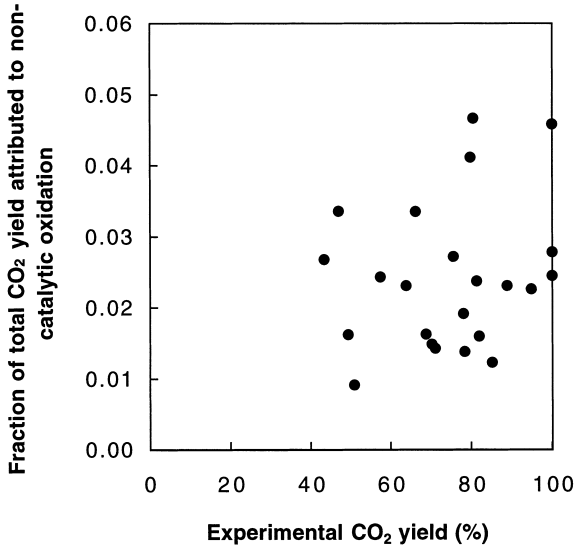

Fig. 1. Fraction of total CO_2 yield determined experimentally that can be attributed to non-catalytic oxidation.

The experimental data in Table 1 clearly show that complete oxidation of phenol to CO_2 is achievable in about 2 s of space time (defined here as the ratio of the catalyst mass to the fluid mass flow rate), which is equivalent to about 1 s of contact time (defined here as the ratio of catalyst bulk volume to fluid volumetric flow rate). That the heterogeneous catalyst effectively increases the reaction rate and promotes complete oxidation to CO_2 is in agreement with previous reports on heterogeneous catalytic SCWO of phenol. While the previous studies reported that the yield of CO_2 reached as high as 90% in 5.4 s of contact time [23,24] and 100% in 15 s [25] at relatively mild temperatures of 390°C, the results here show that complete oxidation of phenol can be achieved in an even shorter time period using the CARULITE 150 catalyst.

4. Mass transport influence

Before using the experimental data to determine the catalytic oxidation kinetics, we first assess the influ-

Table 1
Summary of phenol oxidation experiments over CARULITE 150 at 250 atm

Run	Temperature (°C)	Space time (s)	Phenol concentration (mmol/l)	Oxygen concentration (mmol/l)	Water concentration (mol/l)	Phenol concentration (%)	CO_2 yield (%)	CO yield (%)	Phenol conversion		CO_2 formation	
									k_1 (l/g s)	η	k_1 (l/g s)	η
1	385	0.51	0.720	34.1	19.6	97	80	0.1	0.042	0.47	0.013	0.68
2	384	0.35	1.029	24.8	20.8	88	76	0.4	0.032	0.51	0.017	0.62
3	384	0.25	1.237	18.1	21.4	83	43	0.4	0.042	0.45	0.008	0.76
4	384	0.25	0.831	38.0	22.2	85	66	0.4	0.043	0.44	0.018	0.60
5	383	0.19	1.078	29.8	22.9	74	57	0.5	0.037	0.46	0.018	0.59
6	382	0.17	0.908	39.6	23.7	75	47	0.3	0.046	0.42	0.014	0.63
7	385	0.41	0.762	35.8	20.6	92	80	0.3	0.033	0.50	0.017	0.63
8	384	0.26	1.118	23.2	21.4	80	64	0.4	0.032	0.50	0.016	0.63
9	387	0.79	0.452	36.4	16.8	100	81	0.0			0.009	0.77
10	387	0.58	0.683	27.1	17.0	100	78	0.0			0.012	0.73
11	388	1.81	0.298	38.6	15.5	100	100	0.0				
12	388	1.24	0.575	26.4	15.4	100	95	0.0			0.012	0.75
13	387	0.78	0.890	18.2	17.0	99	85	0.2	0.077	0.39	0.011	0.74
14	387	1.06	0.365	39.1	16.5	100	100	0.0				
15	387	0.76	0.624	28.9	16.7	97	78	0.7	0.039	0.50	0.008	0.79
16	386	0.61	0.784	23.6	17.2	95	71	0.7	0.027	0.58	0.008	0.78
17	387	0.58	1.055	9.60	16.5	94	51	0.4	0.027	0.57	0.005	0.86
18	426	0.40	0.086	17.6	7.22	98	100	2.6	0.030	0.56		
19	417	0.26	0.164	12.3	7.72	82	69	2.2	0.093	0.50	0.053	0.60
20	401	0.20	0.243	11.1	9.44	63	49	1.4	0.054	0.56	0.031	0.66
21	430	0.32	0.070	18.2	7.00	95	89	3.1	0.199	0.39	0.114	0.48
22	425	0.23	0.133	13.3	7.22	84	70	2.5	0.141	0.44	0.075	0.55
23	427	0.20	0.070	18.8	7.17	82	82	3.3	0.162	0.41	0.161	0.41

ence of mass transfer on the observed reaction rate. Mass transfer from the bulk fluid to the catalyst surface (external mass transfer) can limit an observed catalytic reaction rate, as can mass transfer within the pores of the catalyst particle (internal mass transfer). We first determined whether external mass transfer limited the rate of oxidation of phenol under the reaction conditions employed in our experiments. According to Mears' criterion [27], the difference between the concentration of reactant at the catalyst surface and in the bulk fluid (and hence external mass transfer limitation) is insignificant if

$$\frac{(-r'_A)\rho_b d_p}{C_{A0} k_c} < \frac{0.3}{n}. \tag{1}$$

All symbols used in this report are defined in Section 8. By substituting in the expression for the observed catalytic reaction rate

$$-r'_A = \frac{\Delta F_A}{W} = \frac{\dot{m} C_{A0} X}{\rho W} = \frac{C_{A0} X}{\rho \tau'}, \tag{2}$$

the Mears' criterion becomes

$$\frac{X \rho_b d_p}{\rho \tau' k_c} < \frac{0.3}{n}. \tag{3}$$

Among the reactions (runs 1–17 in Table 1) conducted around 385°C, run 6 has the highest value of X/τ', and thus is used in estimating the left-hand side of Eq. (3). The bed density ρ_b and average particle diameter d_p are taken to be 0.8 g/cm^3 and 1.88×10^{-2} cm, respectively. The density (and any other property) of the fluid is approximated as that of the pure water since the concentrations of phenol and oxygen are very low. At 385°C and 250 atm, the density of water ρ is about 0.35 g/cm^3. Thus the final parameter that needs to be evaluated in Eq. (3) is the mass transfer coefficient k_c.

Mass transfer coefficients are usually correlated in the form of a dimensionless Sherwood number as a function of the Schmidt and Reynolds numbers. The correlation given by Wakao and Kaguei [28] for flow through a packed bed is:

$$Sh = 2 + 1.1\, Sc^{1/3}\, Re^{0.6}, \tag{4}$$

where the dimensionless numbers are defined as:

$$Re = \frac{\rho u d_p}{\mu}, \tag{5}$$

$$Sc = \frac{\mu}{\rho D_m}, \tag{6}$$

$$Sh = \frac{k_c d_p}{D_m}. \tag{7}$$

The viscosity of water is estimated from the steam tables [29] as $\mu = 3.8\times 10^{-4}$ g/cm s. Using the slowest flow rate (3 g/s) employed in our experiments, a minimum value of 52 cm/s is estimated for the superficial velocity by

$$u = \frac{4\dot{m}}{\rho \pi D^2}. \tag{8}$$

Thus a minimum value of 900 is estimated for the Reynolds number.

The molecular diffusivity D_m of 9.0×10^{-4} cm^2/s is calculated from a correlation of experimental data for supercritical water [30]:

$$\rho D_m = 2.24 \times 10^{-6}\, T^{0.763}. \tag{9}$$

Combining the viscosity, density and diffusivity, according to Eq. (6) we find the Schmidt number for SCW at 385°C and 250 atm to be $Sc = 1.2$.

These values for Re and Sc lead to a minimum value of 71 for the Sherwood number according to the correlation given in Eq. (4). Consequently, a minimum value of 3.4 cm/s is estimated for the mass transfer coefficient k_c. Our calculation procedure ensures that the highest possible value (worst case) is estimated for the left-hand side of Eq. (3). This value is found to be 0.056, which is clearly less than $0.3/n$ for any reasonable value of the reaction order. Thus, we conclude that external mass transfer did not influence the overall kinetics during our experiments.

Next we considered the effect of the internal mass transfer resistance. The Weisz-Prater parameter [27],

$$C_{wp} = \frac{(-r'_A)\rho_p R^2}{D_e C_{As}} = \frac{C_{A0} X \rho_p d_p^2}{4\rho \tau' D_e C_{As}} \tag{10}$$

is widely used to assess the significance of internal mass transfer limitations on the reaction rate. For first-order reactions, if $C_{wp} \ll 1$, internal mass transfer resistance is not important, whereas if $C_{wp} \gg 1$ there are severe mass transfer limitations on the overall reaction rate.

Most of the data needed to calculate C_{wp} appeared in the discussion of external mass transfer. The

only new data required are ρ_p and D_e. For the CARULITE 150 catalyst, ρ_p is 4.2 g/cm^3. The effective diffusivity D_e of 5.8×10^{-4}cm^2/s is estimated from the molecular diffusion coefficient, the particle porosity ($\epsilon\sim0.8$) and the tortuosity, which can be approximated as the inverse of the porosity [31]:

$$D_e = \frac{\epsilon D_m}{\tau_p} \approx \epsilon^2 D_m. \quad (11)$$

Using the foregoing values, and assuming that C_{As} is roughly equal to C_{A0}, we obtained a C_{wp} value of about 8. Thus it appears that this catalyst is so active that internal mass transfer limits the reaction rate under our experimental conditions. Due to the high activity of the catalyst, all reactions reported here were influenced by internal mass transfer by various degrees. Therefore, the kinetics analysis, which appears in the next section, will include the influence of pore diffusion on the observed experimental results.

5. Kinetics analysis

In light of the internal mass transfer limitation on the kinetics, it was evident that the influence of pore diffusion must be accounted for in any kinetics analysis. We chose to include pore diffusion effects by using the effectiveness factor in our kinetics analysis. The first stage in our analysis was to determine the reaction order. We employ a global power-law rate equation

$$\text{rate of phenol conversion} = k[\text{PhOH}]^a[\text{O}_2]^b \quad (12)$$

to express the rate of phenol conversion, where a and b are the apparent reaction orders for phenol and oxygen. Of course, it is well known that diffusion limitations can disguise the intrinsic reaction order. The reaction order n' determined from experimental data for strongly diffusion-limited reactions differs from the true reaction order n by [27]:

$$n' = \tfrac{1}{2}(1+n). \quad (13)$$

We note, however, that a reaction that is truly first-order will also be first-order with the presence of diffusion limitation.

By combining the design equation for the catalytic isobaric, isothermal, plug-flow reactor

$$\text{rate} = -\frac{dF}{dW} = \frac{\dot{m}[\text{PhOH}]_0\, dX_p}{\rho\, dW} = \frac{[\text{PhOH}]_0\, dX_p}{\rho\, d\tau'} \quad (14)$$

and the power-law rate equation, we obtained Eq. (15):

$$\frac{dX_p}{d\tau'} = \rho k[\text{PhOH}]_0^{a-1}(1-X_p)^a[\text{O}_2]^b. \quad (15)$$

All reactions except for runs 3 and 17 (which were not used in this kinetics analysis) were conducted with at least 180% excess oxygen, so the oxygen concentration was approximated as being conversion invariant and equal to its initial concentration. Thus the differential equation can be solved analytically with the initial condition X_p=0 at τ'=0 to give

$$X_p = 1 - (1-\rho(1-a)k[\text{PhOH}]_0^{a-1}[\text{O}_2]_0^b\tau')^{1/(1-a)} \quad (16)$$

for $a\neq1$.

We performed a non-linear regression analysis to fit the phenol conversions from experiments conducted around 385°C to this model. These 15 data sets (runs 3 and 17 were excluded) led to reaction orders of a=0.94 (±0.09) for phenol, and b=0.29 (±0.19) for oxygen. The numbers in the parentheses represent the 95% confidence interval of the estimated parameters.

Similarly, a consideration of the kinetics for the formation of CO_2, which is equivalent to the rate of disappearance of total organic carbon (TOC), leads to Eq. (17):

$$X_c = 1 - (1-\rho(1-a)k[\text{TOC}]_0^{a-1}[\text{O}_2]_0^b\tau')^{1/(1-a)} \quad (17)$$

for $a\neq1$ where $[\text{TOC}]_0$=6 $[\text{PhOH}]_0$. Again the apparent reaction orders were determined from a non-linear regression of the experimental data around 385°C. The reaction orders in the rate equation for CO_2 formation were found to be a=1.17 (±0.20), and b=0.25 (±0.49). Figs. 2 and 3 compare the experimental phenol and TOC conversions with the values calculated from the rate laws. The reasonably good fit shows that the power-law rate expression provides a reasonable representation of the experimental data.

The apparent reaction orders for phenol in the phenol disappearance rate equation and for TOC in

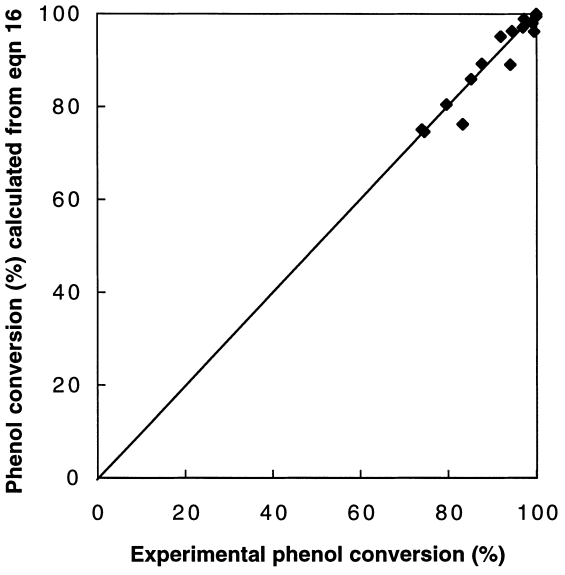

Fig. 2. Parity plot for phenol conversion.

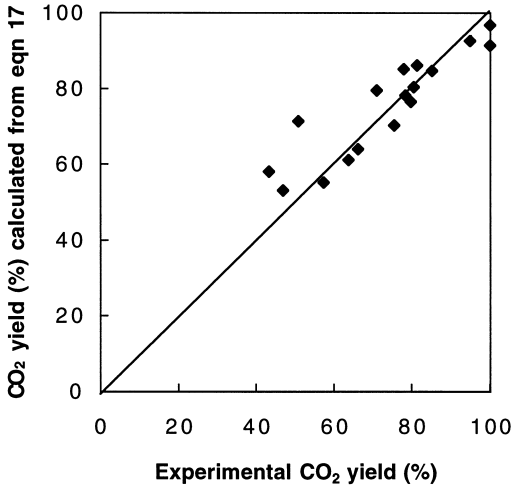

Fig. 3. Parity plot for CO_2 yield.

the CO_2 formation rate law are close to unity, which according to Eq. (13) implies that the true reaction orders are close to unity in both the cases. Meanwhile, the effect of oxygen on the reaction rate is much smaller judging by the lower value but larger uncertainty in the O_2 reaction orders relative to those for phenol and TOC. Thus, it is reasonable to approximate the intrinsic kinetics for both phenol and TOC conversion as following a rate law that is first-order in the organic compound and zero-order in oxygen. The apparent or measurable rate can then be written as

$$\text{apparent rate of phenol conversion} = \eta k_1[\text{PhOH}]. \tag{18}$$

This rate equation includes the effectiveness factor, which accounts for the influence of pore diffusion on the rate. By combining this rate expression with the catalytic reactor design equation Eq. (14) and solving, we obtained Eq. (19):

$$\eta k_1 = \frac{-\ln(1 - X_p)}{\rho\tau'}. \tag{19}$$

Thus we see that the value of the product, ηk_1, can be determined for each run in Table 1.

The effectiveness factor η is a function of the Thiele modulus ϕ. For a first-order reaction,

$$\phi = R\sqrt{\frac{k_1\rho_p}{D_e}}, \tag{20}$$

$$\eta = \frac{3}{\phi^2}(\phi\coth\phi - 1). \tag{21}$$

Since the effectiveness factor is a function of the rate constant as illustrated by Eqs. (20) and (21), we find that Eq. (19) is simply a non-linear equation with one unknown, k_1. Thus, the task of finding both the effectiveness factor and the rate constant for a particular experimental run was reduced to finding the root (rate constant) of Eq. (19). We calculated the rate constants from the experimental data by using the Solver option in Microsoft Excel. Table 1 displays the results of this analysis. Runs 9, 10, 11, 12 and 14 were not used because the phenol conversions were essentially 100%. The effectiveness factors range from 0.38 to 0.58, which confirms the mass transfer limitation on the intrinsic kinetics of phenol conversion during our experiments.

Fig. 4 presents the Arrhenius plot for the phenol disappearance kinetics. The activation energy and pre-exponential factor for phenol disappearance were determined from the linear regression of the data as E_a=30.7 (±7.3) kcal/mol and $A=10^{8.8\ (\pm 2.4)}$ l/g s.

We also used the approach outlined above to evaluate the intrinsic kinetics for the TOC conversion, and the first-order rate constants we obtained appear in Table 1. Fig. 5 presents the Arrhenius plot for TOC

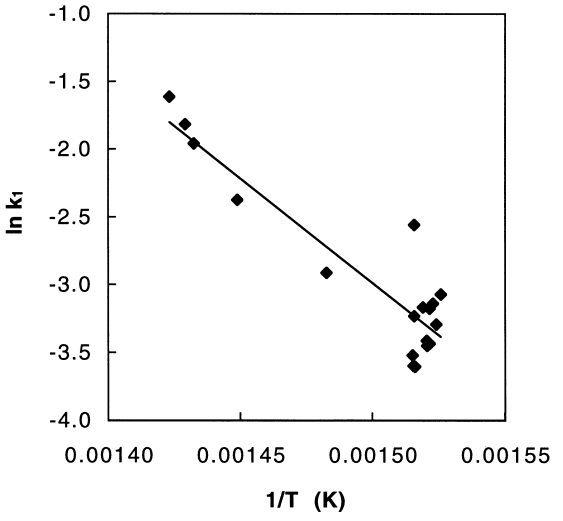

Fig. 4. Arrhenius plot for first-order rate constant for phenol conversion during SCWO.

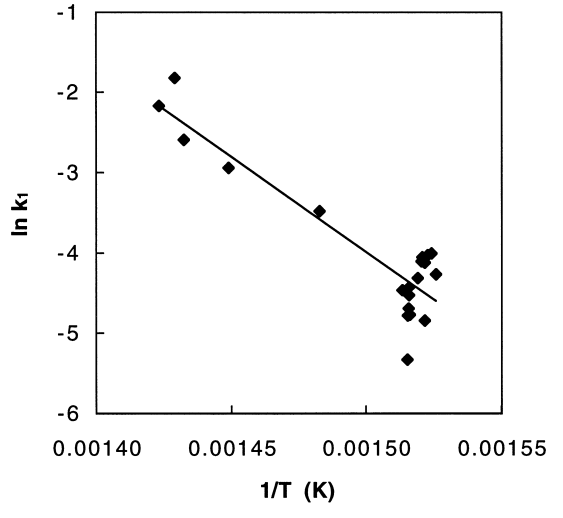

Fig. 5. Arrhenius plot for first-order rate constant for TOC conversion during SCWO.

conversion kinetics. The Arrhenius parameters are E_a=46.9 (±11.1) kcal/mol and $A=10^{13.7\ (\pm 3.6)}$ l/g s.

6. Catalyst deactivation

The experiments listed in Table 1 were conducted with fresh catalysts. In this section experimental data were collected for a catalyst that had already undergone SCWO of phenol for at least two days. We studied the activity change of the catalyst as a function of its age (the time it had been used for SCWO).

Table 2 summarizes three experiments conducted over an aged catalyst under otherwise nearly identical conditions. These conditions are similar to those of run 12 in Table 1. On the basis of the rate laws established in Section 5, we anticipated the phenol conversion and CO_2 yield to be close to 100% and 92%, respectively, for a fresh catalyst. The experimental values in Table 2 are lower than both the calculated values and those of run 12 with fresh catalyst, which indicates that some loss of activity accompanied the aging process. The phenol conversion and CO_2 yield did not decrease further with increasing catalyst age, however, which would be expected if the catalyst underwent persistent, continual deactivation.

The results of a more detailed time-on-stream study of catalyst activity are summarized in Fig. 6. The space time, temperature, pressure, and phenol and O_2 concentrations were maintained close to their initial values throughout the experiment. The catalyst used in this experiment had previously been used for the SCWO of phenol for four days before this experiment began. Thus, the time=0 point does not correspond to fresh catalyst. Throughout three additional days of phenol oxidation, the CO_2 yield fluctuated slightly between 93% and 99%. No significant deac-

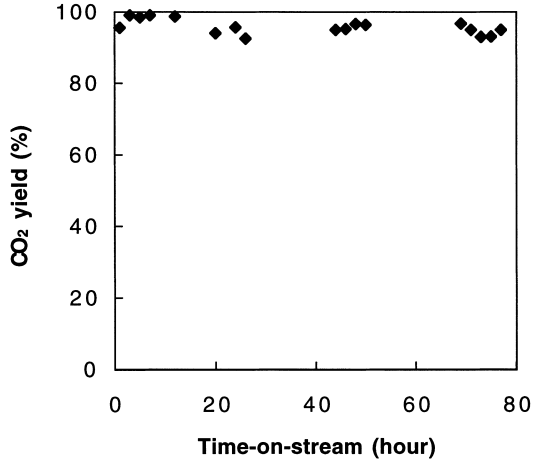

Fig. 6. CO_2 yield from SCWO as a function of time-on-stream ($[PhOH]_0=7\times10^{-4}$ M, $[O_2]_0=4\times10^{-2}$ M, T=385°C, P=250 atm, and τ'=2.8 s).

Table 2
Phenol conversion and CO_2 yield data taken on aged catalyst at 250 atm

Catalyst age (day)	Reaction temperature (°C)	Space time (s)	Phenol concentration (mM)	Oxygen concentration (mM)	CO_2 yield (%)	Calculated CO_2 yield[a] (%)	Phenol conversion (%)	Calculated phenol conversion[b] (%)
2	386	1.21	0.643	30.7	76	95	95	100
4	386	1.29	0.616	31.9	76	95	95	100
7	386	1.21	0.634	31.6	78	95	94	100

[a]From Eq. (17).
[b]From Eq. (16).

tivation of the catalyst was observed throughout this time period. These experimental results show that the CARULITE 150 catalyst maintain a high activity for phenol oxidation in SCW even after several days of continuous operation.

7. Summary and conclusions

The CARULITE 150 catalyst used in this study effectively promotes complete oxidation of phenol under SCWO conditions. The experimental data collected around 385°C were consistent with apparent reaction orders of 0.94 (±0.09) for phenol and 0.29 (±0.19) for oxygen in the power-law rate expression for phenol conversion, and 1.17 (±0.20) for TOC and 0.25 (±0.49) for oxygen in the power-law rate expression for CO_2 formation. Although external mass transfer did not influence the phenol conversion kinetics, the CARULITE 150 catalyst was so active that internal mass transfer did limit the kinetics. A kinetics analysis of the experimental data, which employed first-order rate laws and the internal effectiveness factor, resulted in intrinsic activation energies of 30.7 (±7.3) and 46.9 (±11.1) kcal/mol for the rate constants for phenol conversion and CO_2 formation, respectively. A deactivation study showed that the catalyst maintained its high activity even after several days of continuous operation under SCWO conditions.

8. Notation

C_{A0}	bulk concentration
C_{As}	surface concentration
d_p	particle diameter
D	reactor diameter (ID)
D_m	molecular diffusion coefficient
D_e	effective diffusion coefficient
ϵ	particle porosity
k	rate constant
k_1	first-order rate constant
k_c	external mass-transfer coefficient
$\dot{m}$	mass flow rate
n	intrinsic reaction order
n'	apparent reaction order
P	pressure
R	particle radius
ρ	fluid density
ρ_b	bed density
ρ_p	particle density
τ'	space time ($\tau' = \dot{m}/W$)
τ_p	tortuosity factor
μ	viscosity
u	superficial velocity
W	catalyst mass
X	conversion
Re	Reynolds number
Sc	Schmidt number
Sh	Sherwood number

Acknowledgements

This work was supported by the US Department of Energy (DE-FG22-95PC95213) and the TAPPI Foundation.

References

[1] M. Modell, in: H.M. Freeman (Ed.), Standard Handbook of Hazardous Waste Treatment and Disposal, Section 8.11, McGraw-Hill, New York, 1989.

[2] R. McBrayer, Proceedings of the First International Workshop on Supercritical Water Oxidation, Amelia Island, FL, 6–9 February 1995.
[3] P. Svensson, Chem. Technol. Europe 2 (1995) 16.
[4] T.D. Thornton, P.E. Savage, J. Supercrit. Fluids 3 (1990) 240.
[5] T.D. Thornton, D.E. LaDue, P.E. Savage, Environ. Sci. Technol. 25 (1991) 1507.
[6] T.D. Thornton, P.E. Savage, Ind. Eng. Chem. Res. 31 (1992) 2451.
[7] T.D. Thornton, P.E. Savage, AIChE J. 38 (1992) 321.
[8] R. Li, T.D. Thornton, P.E. Savage, Environ. Sci. Technol. 26 (1992) 2388.
[9] S. Gopalan, P.E. Savage, J. Phys. Chem. 98 (1994) 12646.
[10] S. Gopalan, P.E. Savage, AIChE J. 41 (1995) 1864.
[11] M. Krajnc, J. Levec, AIChE J. 42 (1996) 1977.
[12] S. Imamura, A. Dol, S. Ishida, Ind. Eng. Chem. Prod. Res. Dev. 24 (1985) 75.
[13] S. Imamura, M. Nakamura, N. Kawabata, J. Yoshida, S. Ishida, Ind. Eng. Chem. Prod. Res. Dev. 25 (1986) 34.
[14] S. Imamura, I. Fukuda, S. Ishida, Ind. Eng. Chem. Res. 27 (1988) 718.
[15] J. Levec, M. Herskowitz, J.M. Smith, AIChE J. 22 (1976) 919.
[16] J. Levec, J.M. Smith, AIChE J. 22 (1976) 159.
[17] A. Pintar, J. Levec, J. Catal. 135 (1992) 345.
[18] A. Pintar, J. Levec, Chem. Eng. Sci. 47 (1992) 2395.
[19] A. Pintar, J. Levec, Ind. Eng. Chem. Res. 33 (1994) 3070.
[20] A. Sadana, J.R. Katzer, Ind. Eng. Chem. Fundam. 13 (1974) 127.
[21] A. Sadana, J.R. Katzer, J. Catal. 35 (1974) 140.
[22] D. Mantzavinos, R. Hellenbrand, A.G. Livingston, I.S. Metcalfe, Appl. Catal. 7(B) (1996) 379.
[23] Z.Y. Ding, S.N.V.K. Aki, M.A. Abraham, Environ. Sci. Technol. 29 (1995) 2748.
[24] Z.Y. Ding, M. Frisch, L. Li, E. Gloyna, Ind. Eng. Chem. Res. 35 (1996) 3257.
[25] M. Krajnc, J. Levec, Appl. Catal. 3(B) (1994) L101.
[26] E.F. Gloyna, L. Li, Environ. Prog. 14 (1995) 182.
[27] H.S. Fogler, Elements of Chemical Reaction Engineering, 2nd ed., Prentice-Hall, Englewood Cliffs, NJ, 1992.
[28] N. Wakao, S. Kaguei, Heat and Mass Transfer in Packed Beds, Gordon and Breach, New York, 1982.
[29] L. Haar, J.S. Gallagher, G.S. Kell, NBS/NRC Steam Tables, Hemisphere, New York, 1984.
[30] W.J. Lamb, G.A. Hoffman, J. Jonas, J. Chem. Phys. 74 (1981) 6875.
[31] J.M. Smith, Chemical Engineering Kinetics, McGraw-Hill, New York, 1981.